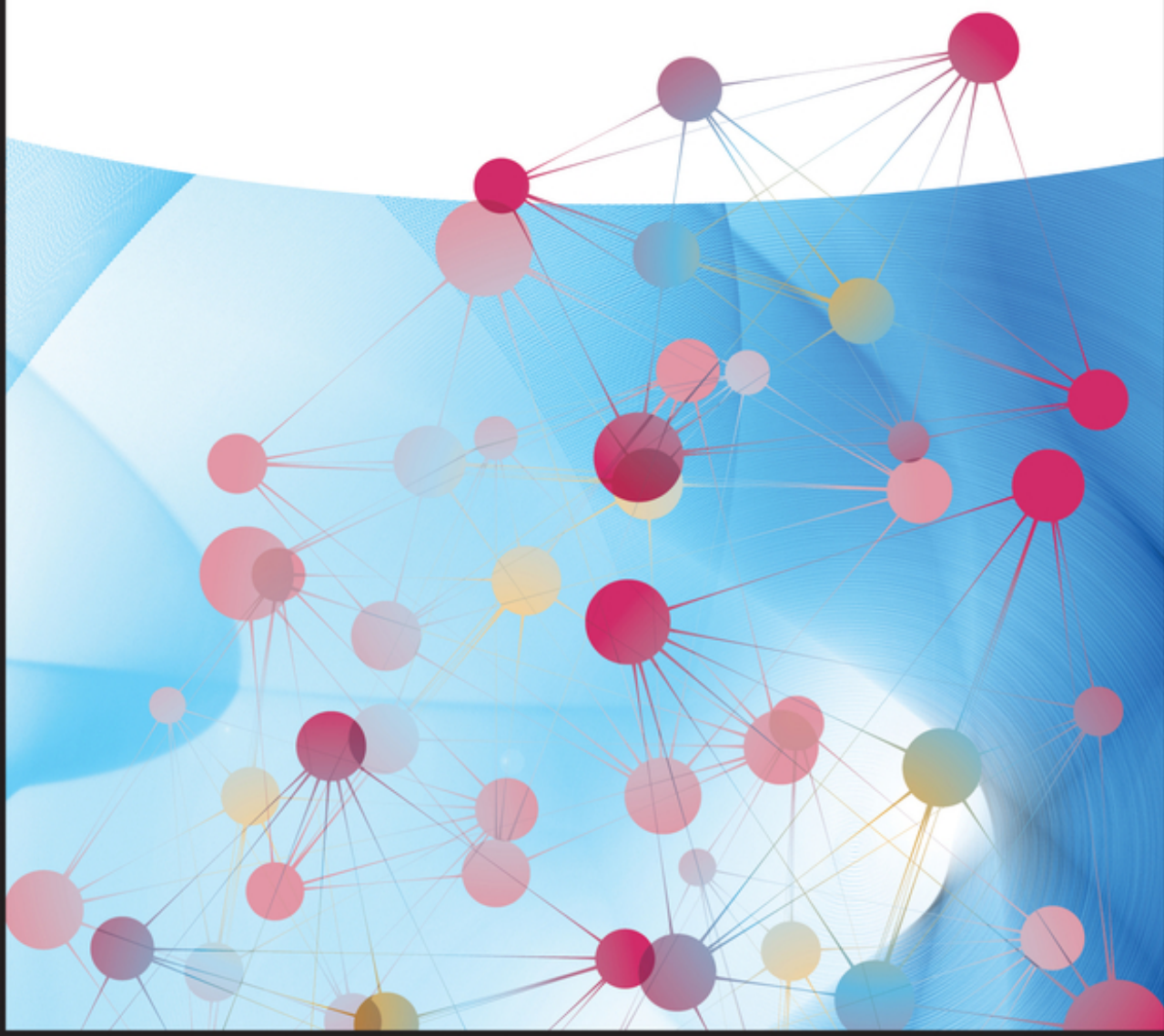


Yoshiaki Nishibayashi

# Transition Metal- Dinitrogen Complexes

Preparation and Reactivity





## Transition Metal-Dinitrogen Complexes



# Transition Metal-Dinitrogen Complexes

Preparation and Reactivity

*Edited by*  
*Yoshiaki Nishibayashi*

**WILEY-VCH**

**Editor**

**Yoshiaki Nishibayashi**  
The University of Tokyo  
School of Engineering  
Hongo, Bunkyo-ku  
113-8656 Tokyo  
Japan

■ All books published by **Wiley-VCH** are carefully produced. Nevertheless, authors, editors, and publisher do not warrant the information contained in these books, including this book, to be free of errors. Readers are advised to keep in mind that statements, data, illustrations, procedural details or other items may inadvertently be inaccurate.

**Library of Congress Card No.:** applied for

**British Library Cataloguing-in-Publication Data**

A catalogue record for this book is available from the British Library.

**Bibliographic information published by the Deutsche Nationalbibliothek**

The Deutsche Nationalbibliothek lists this publication in the Deutsche Nationalbibliografie; detailed bibliographic data are available on the Internet at <<http://dnb.d-nb.de>>.

© 2019 Wiley-VCH Verlag GmbH & Co. KGaA, Boschstr. 12, 69469 Weinheim, Germany

All rights reserved (including those of translation into other languages). No part of this book may be reproduced in any form – by photoprinting, microfilm, or any other means – nor transmitted or translated into a machine language without written permission from the publishers. Registered names, trademarks, etc. used in this book, even when not specifically marked as such, are not to be considered unprotected by law.

**Print ISBN:** 978-3-527-34425-3

**ePDF ISBN:** 978-3-527-34429-1

**ePub ISBN:** 978-3-527-34427-7

**oBook ISBN:** 978-3-527-34426-0

**Typesetting** SPi Global, Chennai, India  
**Printing and Binding**

Printed on acid-free paper

10 9 8 7 6 5 4 3 2 1

## Contents

Preface *xi*

About the Editor *xiii*

- 1**      **Overviews of the Preparation and Reactivity of Transition Metal–Dinitrogen Complexes**    *1*  
*Yoshiaki Tanabe and Yoshiaki Nishibayashi*
- 1.1      Introduction    *1*
- 1.2      Biological Nitrogen Fixation    *4*
- 1.3      Historical Background of Transition Metal–Dinitrogen Complexes    *9*
- 1.4      Coordination Chemistry of Transition Metal–Dinitrogen Complexes    *13*
- 1.4.1    Coordination Patterns of Dinitrogen and Mononuclear Transition Metal–Dinitrogen Complexes    *13*
- 1.4.2    Multinuclear Transition Metal–Dinitrogen Complexes    *16*
- 1.5      Chemical Activation and Reactivity of Dinitrogen Using Transition Metal Complexes    *21*
- 1.5.1    Protonation of Transition Metal-bound Dinitrogen    *21*
- 1.5.2    Cleavage of Transition Metal-bound Dinitrogen    *25*
- 1.5.3    Reaction of Transition Metal-bound Dinitrogen with Dihydrogen    *26*
- 1.5.4    Functionalization of Transition Metal-bound Dinitrogen    *29*
- 1.5.5    Electrochemical and Photochemical Conversion of Dinitrogen Using Transition Metal Complexes    *31*
- 1.6      Catalytic Conversion of Dinitrogen into Ammonia Using Transition Metal Complexes    *34*
- 1.6.1    Catalytic Formation of Ammonia or Hydrazine Using Molybdenum Complexes    *34*
- 1.6.2    Catalytic Formation of Ammonia or Hydrazine Using Transition Metal Other than Molybdenum (Iron, Ruthenium, Osmium, Cobalt, and Vanadium) Complexes    *40*
- 1.6.3    Catalytic Transformation of Hydrazine into Ammonia    *45*
- 1.6.4    Catalytic Formation of Silylamine    *47*
- 1.7      Conclusion and Perspectives    *50*
- References    *51*

<b>2</b>	<b>Group 4 Transition Metal–Dinitrogen Complexes</b>	<b>79</b>
	<i>Hidetake Seino and Yuji Kajita</i>	
2.1	Introduction	79
2.2	Preparation of Group 4 Transition Metal–Dinitrogen Complexes	80
2.2.1	Dinitrogen Complexes of Bis(cyclopentadienyl)titanium Derivatives	80
2.2.2	Dinitrogen Complexes of Bis(cyclopentadienyl)zirconium and Bis(cyclopentadienyl)hafnium Derivatives	89
2.2.3	Other Dinitrogen Complexes Based on Cyclopentadienyl Ligands	98
2.2.4	Dinitrogen Complexes Supported by $\sigma$ -donor Ligands	100
2.2.5	Heterobimetallic Dinitrogen Complexes	109
2.3	Reactions of Group 4 Transition Metal–Dinitrogen Complexes	112
2.3.1	Protonation	112
2.3.2	Reduction	115
2.3.3	Reactions with Hydrogen	120
2.3.4	Reactions with Si–H and B–H Bonds	129
2.3.5	Reactions with Alkyl Halides and Their Equivalents	131
2.3.6	Reactions with Alkynes	136
2.3.7	Reactions with Carbon Dioxide and Cumulenes	138
2.3.8	Reactions with Carbon Monoxide	142
2.3.9	Dinitrogen Ligand Substitution	148
2.4	Conclusion and Perspectives	151
2.5	Addition After Acceptance of this Manuscript	151
	References	152
<b>3</b>	<b>Group 5 Transition Metal–Dinitrogen Complexes</b>	<b>159</b>
	<i>Leila M. Duman and Lawrence R. Sita</i>	
3.1	Introduction	159
3.2	Preparation of Group 5 Metal N <sub>2</sub> Complexes	160
3.2.1	Vanadium	160
3.2.2	Niobium	174
3.2.3	Tantalum	178
3.3	N $\equiv$ N Bond Cleavage Within Group 5 Metal N <sub>2</sub> Complexes	187
3.3.1	Vanadium	188
3.3.2	Niobium	192
3.3.3	Tantalum	197
3.4	Nitrogen Fixation Mediated by Group 5 Transition-metal N <sub>2</sub> Complexes	201
3.4.1	Vanadium	202
3.4.2	Niobium	204
3.4.3	Tantalum	206
3.5	CPAM Group 5 Bimetallic ( $\mu$ - $\eta^1$ : $\eta^1$ -N <sub>2</sub> ) Complexes	206
3.6	Conclusions and Perspectives	212
	References	214



<b>4</b>	<b>Group 6 Transition Metal–Dinitrogen Complexes</b>	<b>221</b>
	<i>Nicolas Mézailles</i>	
4.1	Introduction	221
4.2	Preparation of Group 6 Transition Metal–Dinitrogen Complexes	222
4.2.1	End-on Dinitrogen Complexes from N <sub>2</sub>	222
4.2.1.1	Arene and Phosphine Ligands	222
4.2.1.2	Thioether Ligands	226
4.2.1.3	Nitrogen and Cp Ligands	226
4.2.2	End-on Bridging Dinitrogen Complexes from N <sub>2</sub> : Synthesis and N <sub>2</sub> Splitting	228
4.3	Stoichiometric Reactions of Group 6 Transition Metal–Dinitrogen and Metal–Nitrido Complexes	234
4.3.1	N–H Bond Formation	234
4.3.2	N–C Bond Formation	238
4.3.3	N–element Bond Formation	241
4.4	Catalytic Reactions of Group 6 Transition Metal–Dinitrogen Complexes	247
4.4.1	Catalytic Formation of N <sub>2</sub> H <sub>4</sub> /NH <sub>3</sub> from Nonisolated M–N <sub>2</sub> Complexes	247
4.4.2	Catalytic Formation of N(SiMe <sub>3</sub> ) <sub>3</sub>	247
4.4.3	Catalytic Formation of NH <sub>3</sub>	251
4.5	Chemistry of Cr Complexes	259
4.6	Conclusion and Perspectives	261
	References	263
<b>5</b>	<b>Toward N–N Bond Cleavage: Synthesis and Reactivity of Group 7 Dinitrogen Complexes</b>	<b>271</b>
	<i>Elon A. Ison</i>	
5.1	Synthesis of Group VII N <sub>2</sub> Complexes	271
5.1.1	Syntheses of Terminal N <sub>2</sub> Complexes	271
5.1.2	Reactivity of Terminal N <sub>2</sub> Complexes	275
5.1.2.1	Synthesis of Bridged N <sub>2</sub> Complexes by Reaction with Lewis Acids	276
5.1.2.2	Alternative Syntheses of Bridged N <sub>2</sub> Complexes	279
5.2	Cleavage and Functionalization of N <sub>2</sub> Bonds	280
5.2.1	Generation of Diazomethane from CpMn(CO) <sub>2</sub> N <sub>2</sub>	280
5.2.2	Cleavage of N <sub>2</sub> in the Coordination Sphere of Rhenium	281
5.3	Conclusions and Future Outlook	281
	References	282
<b>6</b>	<b>Group 8 Transition Metal–Dinitrogen Complexes</b>	<b>285</b>
	<i>Adam D. Piascik and Andrew E. Ashley</i>	
6.1	Introduction	285
6.2	Preparation of Group 8 Transition Metal–Dinitrogen Complexes	288
6.2.1	Ligand Substitution	288
6.2.2	Precursor Reduction	292
6.2.3	Other Methods	296

- 6.3 Stoichiometric Reactions of Group 8 Transition Metal–Dinitrogen Complexes 297
  - 6.3.1 Substitution Reactions and Lability of Bound  $N_2$  297
  - 6.3.2 Cleavage and Functionalization of Coordinated  $N_2$  301
  - 6.3.3 Other Stoichiometric Reactivity 309
- 6.4 Catalytic Reactions of Group 8 Transition Metal–Dinitrogen Complexes 311
  - 6.4.1 Early Results and Fe Bis(diphosphine) Systems for Catalytic  $N_2$  Fixation 311
  - 6.4.2 Catalytic  $NH_3$  Production by  $EP^R_3$ -supported Systems 313
  - 6.4.3 Catalytic  $N_2$  Fixation by Other Systems 317
  - 6.4.4 Other Catalytic Reactions of Group 8  $M-N_2$  Complexes 319
- 6.5 Conclusion and Perspectives 327
- References 328
  
- 7 Group 9 Transition Metal–Dinitrogen Complexes 337**  
*Connie C. Lu and Steven D. Prinslow*
  - 7.1 Cobalt–Dinitrogen Complexes 337
    - 7.1.1 Monodentate Phosphine Donors 338
      - 7.1.1.1  $CoH(N_2)(PR_3)_3$  and Related Co(I) Complexes 338
      - 7.1.1.2 Cobaltate Complexes:  $[Co(N_2)(PR_3)_3]^-$  342
    - 7.1.2 Tripodal Polyphosphine Ligands 345
      - 7.1.2.1 Tris(phosphine) Ligands 345
      - 7.1.2.2 Tris(phosphino)borate Ligands 346
      - 7.1.2.3 Trisphosphine Systems with an Apical Main Group Donor 347
      - 7.1.2.4 Trisphosphine Systems with an Apical Transition Metalloligand Donor 350
    - 7.1.3 Ligands with Exclusively Nitrogen Donors 355
      - 7.1.3.1 Tris(pyrazoyl)borate (Tp) Ligands 355
      - 7.1.3.2  $\beta$ -diketimate Ligands 356
      - 7.1.3.3 Bis( $\alpha$ -imino)pyridine Ligands 358
    - 7.1.4 *N*-heterocyclic Carbene Ligands 359
    - 7.1.5 Pincer Ligands 360
      - 7.1.5.1 Monoanionic PNP-Type and PBP-Type Ligands 361
      - 7.1.5.2 Pincer Ligands with N/P Donors 363
      - 7.1.5.3 *N*-heterocyclic Carbene-Based Pincer Ligands 365
    - 7.1.6 Other Assorted Ligands 367
    - 7.1.7 Analysis and Summary of Cobalt–Dinitrogen Complexes 369
  - 7.2 Rhodium–Dinitrogen Complexes 370
    - 7.2.1 Early Rh– $N_2$  Complexes 370
    - 7.2.2 Phosphine Ligands 372
    - 7.2.3 Ligands with Exclusively Nitrogen Donors 374
      - 7.2.3.1 Bis( $\alpha$ -imino)pyridine Ligands 374
      - 7.2.3.2  $\beta$ -diketimate Ligands 375
    - 7.2.4 Pincer Ligands 375
      - 7.2.4.1 PCP Pincer Ligands 376
      - 7.2.4.2 PNP Pincer Ligands 378

7.2.4.3	Other Pincer Ligands	380
7.2.5	<i>N</i> -heterocyclic Carbene Ligands	380
7.2.6	Summary of Rhodium–Dinitrogen Complexes	381
7.3	Iridium–Dinitrogen Complexes	381
7.3.1	Early Ir–N <sub>2</sub> Complexes	382
7.3.2	Phosphine Ligands	383
7.3.3	Ligands with Exclusively Nitrogen Donors	385
7.3.3.1	Tris(pyrazoyl)borate (Tp) Ligands	385
7.3.3.2	β-diketimate Ligands	386
7.3.4	Pincer Ligands	386
7.3.4.1	PNP-Type Pincer Ligands	386
7.3.4.2	PCP- and PSiP-Type Pincer Ligands	388
7.3.5	<i>N</i> -heterocyclic Carbene Ligands	390
7.3.6	Miscellaneous	391
7.3.7	Summary of Iridium–Dinitrogen Complexes	391
7.4	Group 9 Catalysts for N <sub>2</sub> Functionalization	392
7.4.1	Cobalt-Based Catalysts	392
7.4.1.1	Dinitrogen Silylation	393
7.4.1.2	Dinitrogen Fixation	395
7.4.2	Outlook for Rhodium and Iridium Catalysts	396
	Acknowledgments	396
	References	396
<b>8</b>	<b>Group 10 and 11 Transition Metal–Dinitrogen Complexes</b>	<b>403</b>
	<i>Ricardo B. Ferreira and Leslie J. Murray</i>	
8.1	Introduction	403
8.2	Group 10 Transition Metal–Dinitrogen Complexes	405
8.2.1	Nickel	405
8.2.1.1	Interaction of Dinitrogen with Nickel Surfaces	406
8.2.1.2	Matrix-Assisted Isolation of Binary or Ternary Compounds	406
8.2.1.3	Coordination Compounds	408
8.2.1.4	Structural Relationships and Comparisons	420
8.2.2	Palladium and Platinum	422
8.3	Group 11 Transition Metal–Dinitrogen Complexes	423
8.3.1	Copper	423
8.3.1.1	Matrix-Assisted Isolation of Binary or Ternary Compounds	423
8.3.1.2	Coordination Compounds	425
8.3.1.3	Structural Relationships and Comparisons	427
8.3.2	Silver and Gold	429
8.4	Conclusion and Perspectives	430
	References	431
<b>9</b>	<b>Group 3 Transition Metal, Lanthanide, and Actinide–Dinitrogen Complexes</b>	<b>441</b>
	<i>Yoshiaki Tanabe</i>	
9.1	Introduction	441

9.2	Preparation and Characterization of Group 3 Transition Metal, Lanthanide, and Actinide–Dinitrogen Complexes	443
9.2.1	Overviews of Preparation, Structures, and Characterization of Group 3 Transition Metal, Lanthanide, and Actinide–Dinitrogen Complexes	443
9.2.2	Preparation and Structures of Side-on-Bound $\{(N_2)^{2-}\}$ -Bridged Dinuclear Group 3 Transition Metal, Lanthanide, and Actinide–Dinitrogen Complexes	443
9.2.3	Preparation and Structures of Side-on-bound $\{(N_2)^{3-}\}$ -Bridged Dinuclear Group 3 Transition Metal and Lanthanide Complexes	456
9.2.4	Preparation and Structures of $\{(N_2)^{4-}\}$ -Bridged Dinuclear, Trinuclear, and Tetranuclear Lanthanide and Actinide–Dinitrogen Complexes	457
9.2.5	Preparation and Structures of End-on-Bound Group 3 Transition Metal, Lanthanide, and Actinide–Dinitrogen Complexes	460
9.3	Reactivity and Property of Group 3 Transition Metal, Lanthanide, and Actinide–Dinitrogen Complexes	462
9.3.1	Cleavage, Protonation, and Functionalization of Dinitrogen upon Group 3 Transition Metal, Lanthanide, and Actinide–Dinitrogen Complexes	462
9.3.2	Group 3 Transition Metal–Dinitrogen Complexes as Mediators for the Transformation of Small Molecules	466
9.3.3	$\{(N_2)^{3-}\}$ -Bridged Dinuclear Group 3 Transition Metal and Lanthanide Complexes as Single-Molecule Magnets	468
9.4	Conclusion and Perspectives	469
	References	470
	<b>Index</b>	475

## Preface

A great progress has recently been achieved in the research area of Nitrogen Fixation, as one of the most important subjects in chemistry. Especially, the development of catalytic ammonia formation from nitrogen gas under mild reaction conditions has been repowered by several research groups. Although nitrogen fixation chemistry is one of the most notable fields of research, books provide comprehensive knowledge of the relevant fields are rather limited until now. I believe that the latest research results by researchers engaged in state-of-the-art research on synthesis of transition metal–dinitrogen complexes and their reactivity in this book will give very useful information to researchers, teachers, and students who are interested in the research field of nitrogen fixation by using transition metal–dinitrogen complexes.

I would like to thank all the contributors for their chapters in this book and their enthusiastic efforts to present recent advances of Nitrogen Fixation by using transition metal–dinitrogen complexes. I anticipate that their contributions will stimulate further study in Nitrogen Fixation. I would like also to offer my warm thanks to the Wiley-VCH team for their continuous support. Finally, I deeply appreciate staffs and students in my research group for their valuable assistances.

May 2018

*Yoshiaki Nishibayashi*  
The University of Tokyo  
School of Engineering  
Tokyo, Japan



## About the Editor

**Yoshiaki Nishibayashi** is a full professor at the University of Tokyo, since 2016. He received his PhD in 1995 from Kyoto University under the supervision of Professor Sakae Uemura. He became an assistant professor at the University of Tokyo in 1995 and moved to Kyoto University in 2000. In 2005, he became an associate professor at the University of Tokyo as PI. Since 2016, he has been a full professor at the University of Tokyo. He received the Chemical Society of Japan Award for Distinguished Young Chemists in 2001, the Minister Award for Distinguished Young Scientists Japan in 2005, the JSPS Prize in 2012, the Green & Sustainable Chemistry Honorable Award in 2012, the Nissan Chemical Industries Award for Novel Reaction & Method from the Society of Synthetic Organic Chemistry, Japan in 2016, the Japan Society of Coordination Chemistry Award for Creative Work in 2017, the Inoue Prize for Science in 2018, and the Prizes for Science and Technology (Research Category) in the Commendation for Science and Technology by the Minister of Education, Culture, Sports, Science, and Technology in 2018. His current research interests are focused on organic and organometallic chemistry. He is the author of more than 200 publications and review articles.





# Overviews of the Preparation and Reactivity of Transition Metal–Dinitrogen Complexes

Yoshiaki Tanabe and Yoshiaki Nishibayashi

Department of Systems Innovation, School of Engineering, The University of Tokyo, Hongo, Bunkyo-ku, Tokyo 113-8656, Japan

## 1.1 Introduction

Nitrogen, the fifth most abundant element in the solar system, is the most abundant element in the atmosphere of Earth [1] as well as the fourth most abundant element in cellular biomass [2]. However, it is rather a trace element in the lithosphere of Earth [3]. Thus, utilization of chemically inert gaseous molecular dinitrogen ( $\text{N}_2$ ) that exists in the atmosphere of Earth as the primary nitrogen source is inevitable in both biogeography and industry. Indeed, fixation of atmospheric nitrogen can be achieved by the conversion of molecular dinitrogen into ammonia ( $\text{NH}_3$ ) containing the most reduced form of nitrogen (–3) that can be a convenient precursor for several nitrogen-containing compounds and has been the most fundamental reaction pathway of the global nitrogen cycle [4, 5]. Industrially,  $\text{NH}_3$  is one of the 10 largest commodity chemical products and has been produced by the Haber–Bosch process in which atmospheric dinitrogen reacts with gaseous dihydrogen ( $\text{N}_2 + 3 \text{H}_2 \rightarrow 2 \text{NH}_3$ ) since the early twentieth century [6–14]. Haber and van Oordt in 1904 first succeeded in the conversion of the mixture of  $\text{N}_2$  and  $\text{H}_2$  into  $\text{NH}_3$  in the presence of transition metal catalyst (Fe or Ni) at a high temperature in a laboratory [15–17]. Later, modification of the reactors and catalysts was achieved, and 90 g of ammonia was shown to be obtained every hour by using an osmium-based catalyst with the total yield of ammonia up to 8 vol% at 550 °C and a total pressure of 175 atm of a stoichiometric mixture of dinitrogen and dihydrogen (1 : 3) in an experimental lecture held in Karlsruhe on 18 March 1909 [18–20]. Further modification of the catalysts for industrialization was investigated by Mittasch and coworkers in BASF, leading to the discovery of the combination of iron,  $\text{K}_2\text{O}$ , and  $\text{Al}_2\text{O}_3$  as one of the most active catalysts by 1910 [6, 21]. The first commercial plant for ammonia synthesis at Oppau began its operation by 1913 in collaboration with Bosch and coworkers at BASF, while the earlier commercial methods to fix atmospheric nitrogen such as Frank–Caro cyanamide process ( $\text{CaC}_2 + \text{N}_2 \rightarrow \text{CaCN}_2 + \text{C}$ ) and Birkeland–Eyde electric arc process ( $\text{N}_2 + \text{O}_2 \rightarrow 2 \text{NO}$ ) were gradually replaced by the Haber–Bosch ammonia process [6–14]. Typical reaction conditions of the Haber–Bosch process are

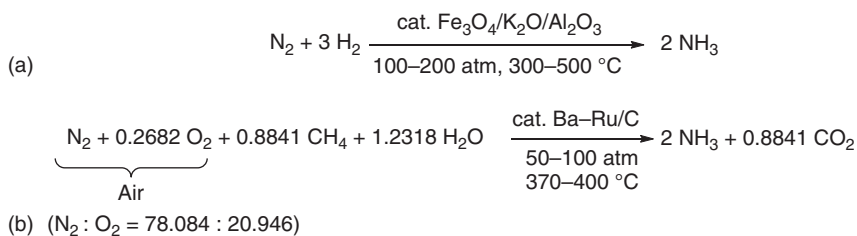


**Figure 1.1** (a) Prototype Haber–Bosch process operated at the first BASF’s Oppau plant. H<sub>2</sub> is originally obtained from steam reforming of coal. (b) Kellogg advanced ammonia process with methane steam reforming.

shown in Figure 1.1a [6], where the reaction is carried out under high temperature and high pressure in the presence of heterogeneous solid-state catalysts prepared from magnetite (Fe<sub>3</sub>O<sub>4</sub>) with the addition of alumina (Al<sub>2</sub>O<sub>3</sub>), silica (SiO<sub>2</sub>), or alkaline earth metal oxide (CaO) as a “structural” promoter and alkaline metal oxide (K<sub>2</sub>O) as an “electronic” promoter.

Although formation of NH<sub>3</sub> from N<sub>2</sub> and H<sub>2</sub> is thermodynamically favored under standard conditions ( $\Delta_r H^\circ = -45.90 \text{ kJ mol}^{-1}$ ,  $\Delta_r G^\circ = -16.37 \text{ kJ mol}^{-1}$  at 1 bar and 25 °C), this conversion can hardly occur at ambient reaction conditions because the dissociation energy of the dinitrogen triple bond is high ( $D_0^\circ = 945.37 \text{ kJ mol}^{-1}$ ) [22]. To lower and surmount the activation energy of this conversion, elevated pressure and temperature as well as heterogeneous solid-state catalysts are necessary, where bond-breakings upon chemisorption on the surface of solid-state catalysts were experimentally observed by Ertl and coworkers, who clarified the surface reaction pathway of the Haber–Bosch process as shown in Figure 1.2 [23–29]. Activation energy and turnover frequency of the catalytic ammonia synthesis are highly dependent not only on the catalyst but also on temperature, pressure, and the ratio of the substances and products, where the logarithm of the equilibrium constant for the reaction of  $\text{N}_2 + 3 \text{H}_2 = 2 \text{NH}_3$  at 1 bar becomes zero theoretically at 456 K [22]. For example, the apparent activation energy for the catalytic ammonia synthesis on the Fe(111) surface of an iron single crystal at around 748 K and a total pressure of 20 atm of a stoichiometric mixture of dinitrogen and dihydrogen (1 : 3) was determined by Somorjai and coworkers as  $81.2 \text{ kJ mol}^{-1}$  with an initial turnover frequency of  $12.7 \pm 2.0$  molecules of ammonia per C<sub>4</sub> surface iron atom per second [30].

A more improved method such as Kellogg advanced ammonia process (KAAP) uses ruthenium-based catalyst supported on graphite-containing carbon copromoted with barium, cesium, or rubidium performed at comparably lower pressure and temperature, the stoichiometry of which can be expressed as Figure 1.1b, when natural gas steam reforming is applied to ammonia production without the separation of dinitrogen from air [8–14, 31–35]. In this reaction, methane is the main hydrogen source of ammonia, and the gaseous ammonia obtained from the stoichiometry in Figure 1.1b theoretically contains 20.8 GJ per metric ton or  $355 \text{ kJ mol}^{-1}$  as chemical energy calculated based on the heat of combustion of methane in the lower heating value (LHV) ( $\Delta_c H^\circ = -802.3 \text{ kJ mol}^{-1}$ ,  $\Delta_c G^\circ = -800.8 \text{ kJ mol}^{-1}$ ) or 18.6 GJ per metric ton

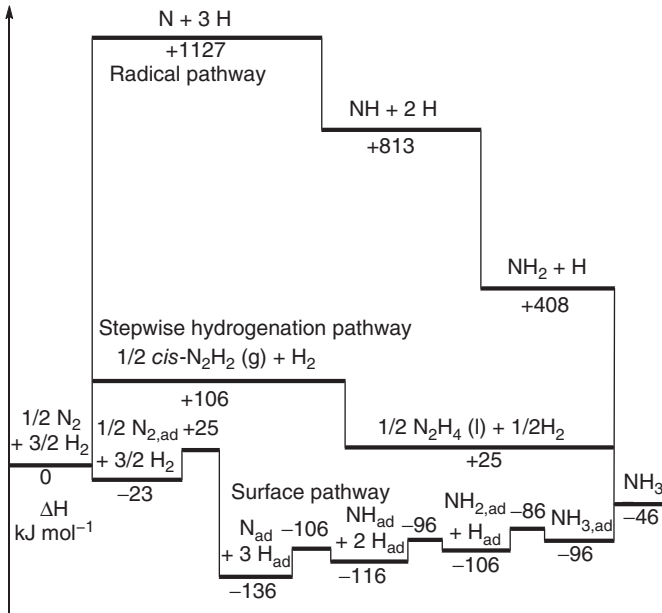


**Figure 1.2** Potential energy diagram for ammonia synthesis on the surface of iron, via stepwise hydrogenation or via formation of radicals.

based on that of ammonia ( $\Delta_c H^\circ = -316.8 \text{ kJ mol}^{-1}$ ,  $\Delta_c G^\circ = -326.5 \text{ kJ mol}^{-1}$ ) if full recovery of the reaction heat is assumed ( $\Delta_r H^\circ = -37.8 \text{ kJ mol}^{-1}$  and  $\Delta_r G^\circ = -27.5 \text{ kJ mol}^{-1}$  per  $\text{NH}_3$  for Figure 1.1b) [22]. A classical BASF-type Haber–Bosch process that uses coke consumes chemical energy of 100 GJ per metric ton of  $\text{NH}_3$  in 1920 [6], which is much more efficient than the Birkeland–Eyde electric arc process (600 GJ per metric ton of fixed nitrogen) or the Frank–Caro cyanamide process (190 GJ per metric ton of  $\text{NH}_3$  derived from the decomposition of  $\text{CaCN}_2$  with  $\text{H}_2\text{O}$ ) [12], whereas the most efficient ammonia plant with the ruthenium-based catalyst and methane steam reforming consumes as low as 27.2 GJ per metric ton or  $463 \text{ kJ mol}^{-1}$  of  $\text{NH}_3$ , where energy efficiency of around 75% with respect to the stoichiometric methane demand is achieved, which also means that additional chemical energy of  $108 \text{ kJ mol}^{-1}$  is required for the industrial synthesis of  $\text{NH}_3$  as represented in Figure 1.1b [13]. In an exergy analysis of a low-energy ammonia process to obtain the liquefied ammonia at  $-33^\circ \text{C}$  (20.14 GJ per metric ton or  $343 \text{ kJ mol}^{-1}$ ) by Dybkjaer under a model reaction at  $140 \text{ kgf cm}^{-2}$  in an indirectly cooled two-bed radial converter using pure methane, cooling water available at  $30^\circ \text{C}$ , a steam to the carbon ratio of 2.5, and so forth, a total exergy of 30.69 GJ per metric ton or  $523 \text{ kJ mol}^{-1}$  is consumed with an exergy loss of 10.55 GJ per metric ton or  $180 \text{ kJ mol}^{-1}$  corresponding to a thermodynamic efficiency of 66% for the production of  $\text{NH}_3$ , where the biggest loss of exergy occurs at methane steam reforming sections with rather a slight loss made during the actual ammonia synthesis ( $1.70 \text{ GJ per metric ton}$  or  $29 \text{ kJ mol}^{-1}$ ) [13, 36]. Further improvement of Haber–Bosch catalysts is still in progress, especially in the development of electronic and structural promoters. For example, Hosono and coworkers have

developed ruthenium-loaded electrode catalysts, which show higher catalytic performance than the conventional ruthenium catalysts at lower temperatures and pressures [37–40].

In total, the Haber–Bosch process annually produces more than 170 million metric tons of  $\text{NH}_3$  [41], consumes fossil fuels as the hydrogen source of  $\text{NH}_3$ , corresponding to 1–2% of the world's annual primary energy supply, and is responsible for the emission of more than 450 million metric tons of  $\text{CO}_2$  [42–44]. This pollution can be reduced by using renewable energy sources for producing dihydrogen from water, but it should be more convenient to use water as a proton source for ammonia without using dihydrogen gas in high pressure and temperature.

It must be noted that ammonia is attracting attention as a possible hydrogen carrier in the future, as well as a fuel for vehicles [45–49], which can minimize the use of fossil fuels. The present Haber–Bosch process requires a lot of reactors to obtain high pressure and temperature; thus, biological nitrogen fixation that can be carried out in small cells at ambient reaction conditions by using water as a proton source has been investigated as a model of an alternative method for the Haber–Bosch process [50–54].

## 1.2 Biological Nitrogen Fixation

Atmospheric molecular dinitrogen has been fixed as ammonia via biological nitrogen fixation using electron carriers (ferredoxins or flavodoxins) as reducing reagents and water as a proton source under ambient pressure and temperature by some specific bacterial and archaeal organisms that possess nitrogen-fixing enzyme called nitrogenase [51, 52]. Based on the difference in transition metal (Mo, V, or Fe) included in its key cofactor (iron–molybdenum cofactor (FeMo-co), iron–vanadium cofactor (FeV-co), or iron–iron cofactor (FeFe-co)) consisting of an iron–sulfur cluster, nitrogenase can be classified into molybdenum nitrogenase, vanadium nitrogenase, or iron-only nitrogenase, among which molybdenum nitrogenase, the canonical form of this enzyme, works most efficiently, where 8 equiv of electrons and protons is consumed for reducing 1 equiv of dinitrogen to form 2 equiv of ammonia together with the formation of an equimolar amount of dihydrogen gas (Figure 1.3a), whereas vanadium nitrogenase (Figure 1.3b) or iron-only nitrogenase (Figure 1.3c) is less effective requiring more protons and electrons wasted to form more dihydrogen molecules [55, 56]. All the diazotrophic bacteria known to date encode molybdenum nitrogenase, whereas some diazotrophic bacteria especially living in soils possess the genes for alternative vanadium or iron-only nitrogenase. Few species such as *Azotobacter vinelandii*, an aerobic free-living microorganism in soils, are known to contain all the three types of nitrogenases, but utilization of alternative vanadium or iron-only nitrogenase occurs under molybdenum limitation or both molybdenum and vanadium limitations, respectively [57–59].

Structures of FeMo-co (Figure 1.4a) and FeV-co (Figure 1.4b) are determined both crystallographically and spectroscopically, where  $\text{Fe}_4\text{S}_3$  and  $\text{Fe}_3\text{MS}_3$  ( $\text{M} = \text{Mo}$  or  $\text{V}$ ) cuboidal units share one central carbon atom, and are further

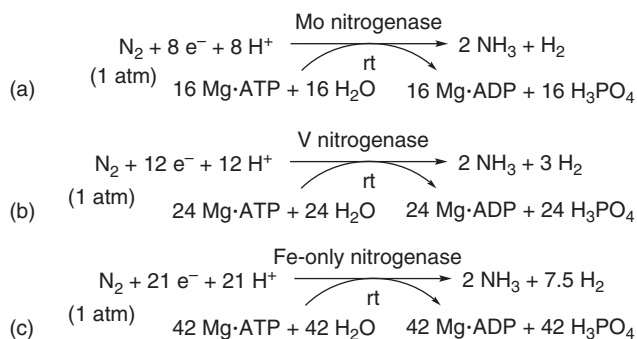


**Figure 1.3** Proposed stoichiometry of biological nitrogen fixation by three types of nitrogenases: (a) molybdenum nitrogenase, (b) vanadium nitrogenase, and (c) iron-only nitrogenase.

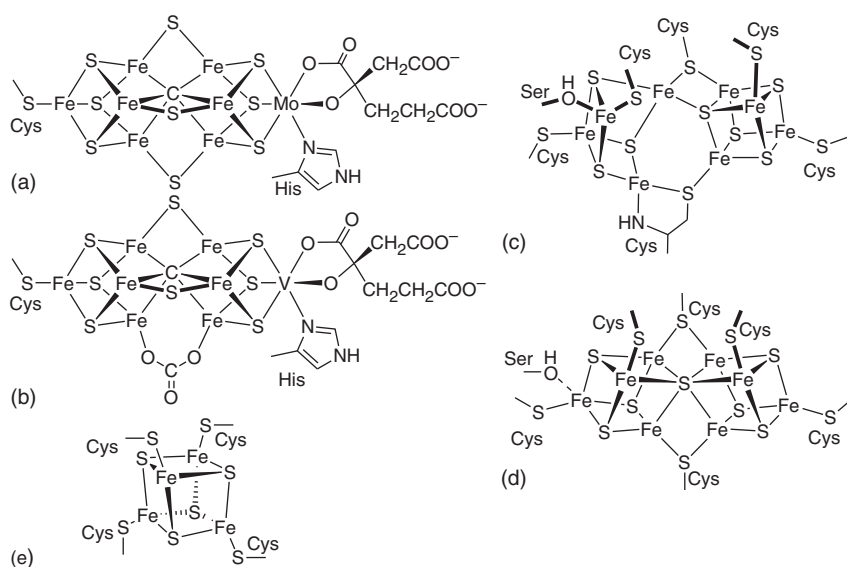


**Figure 1.4** Structures of (a) FeMo-co in MoFe protein, (b) FeV-co in VFe protein, (c) P-cluster in the oxidized state in MoFe protein, (d) P-cluster in the reduced state in MoFe protein, and (e) [4Fe-4S] cluster in Fe protein.

bridged by three sulfur atoms for FeMo-co [60–62] or a combination of two sulfur atoms and one carboxylate for FeV-co [63], respectively. The structure of FeFe-co has not yet been determined crystallographically but has been spectroscopically supposed to have a similar structure to FeMo-co or FeV-co, where molybdenum or vanadium atom is substituted for the corresponding iron atom [51, 52]. As shown in Figure 1.4a,b, molybdenum and vanadium atoms are coordinatively saturated by the chelation of homocitrate, whereas the iron atoms surrounding the carbon atom have vacant sites. Thus, recent theories on the reaction mechanism of nitrogen fixation prefer coordinatively unsaturated iron atoms to molybdenum or vanadium atom where conversion of dinitrogen

into ammonia occurs, whereas the precise reaction pathways for the conversion of dinitrogen into ammonia remain arguable [64–72].

Thermodynamic favorability of the formation of ammonia in aqueous solution changes depending on the pH of the solution because proton transfers are involved in the reaction, and ammonia exists as an ammonium cation ( $pK_a = 9.25$ ) in acidic or neutral conditions. Standard transformed Gibbs energy of the reaction of dinitrogen, electrons, and protons to form ammonium cation and dihydrogen in a ratio of 2:1 in an aqueous solution is given as  $-159.7 \text{ kJ mol}^{-1}$  per dinitrogen at pH 0 ( $a_{\text{H}^+} = 1$ ) and zero ionic strength, which corresponds to standard electrode potential of  $+0.276 \text{ V}$ . On the other hand, standard transformed Gibbs energy at pH 7 shifts to  $+239.8 \text{ kJ mol}^{-1}$ , corresponding to standard apparent reduction potential of  $-0.311 \text{ V}$  vs. SHE (standard hydrogen electrode) (Figure 1.5a) [73]. Thus, the reaction requires the introduction of appropriate reducing reagents such as ferredoxin ( $E'^\circ$  value varies from  $-0.377$  to  $-0.434 \text{ V}$  at pH 7 from different biological sources) (Figure 1.5b) [74, 75] and hydrolysis of several ATPs (ATP = adenosine triphosphate; Figure 1.5c) [75–77].

The schematic shown in Figure 1.6 summarizes the key metabolic pathways related to nitrogen fixation by molybdenum nitrogenase, which consists of two component proteins: molybdenum–iron protein also called dinitrogenase or nitrogenase component 1 containing FeMo-co and P-cluster whose structures in different oxidation states are shown in Figure 1.4c,d [78] and iron protein also called dinitrogenase reductase or nitrogenase component 2 containing [4Fe–4S] cluster whose structure is shown in Figure 1.4e [79, 80]. An electron is transferred from ferredoxin or flavodoxin to the [4Fe–4S] cluster in iron protein, which docks with the aid of 2 M amount of ATP to molybdenum–iron protein to

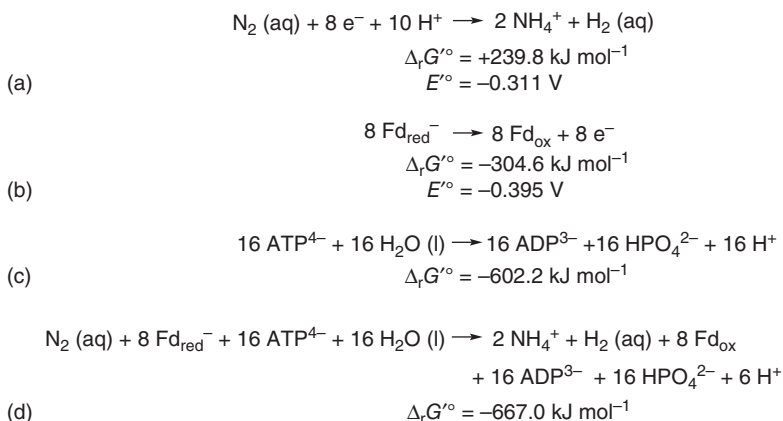


**Figure 1.5** Standard transformed Gibbs energies and standard apparent reduction potentials of reactions in molybdenum nitrogenase at 25 °C, 0 ionic strength, and pH 7: (a) nitrogen fixation, (b) reduction of ferredoxin (reduction potential based on the data obtained from *Clostridium pasteurianum*), (c) hydrolysis of ATP, and (d) total reactions. Stoichiometry in (c) and (d) is shown ignoring  $\text{HATP}^{3-}$  ( $pK_a = 7.60$ ),  $\text{HADP}^{2-}$  ( $pK_a = 7.18$ ), and  $\text{H}_2\text{PO}_4^-$  ( $pK_a = 7.22$ ), but thermodynamic data in (c) and (d) are calculated considering these equilibria at pH 7 (not 16  $\text{H}^+$  but 11.9  $\text{H}^+$  for (c), not 6  $\text{H}^+$  but 1.9  $\text{H}^+$  for (d)).

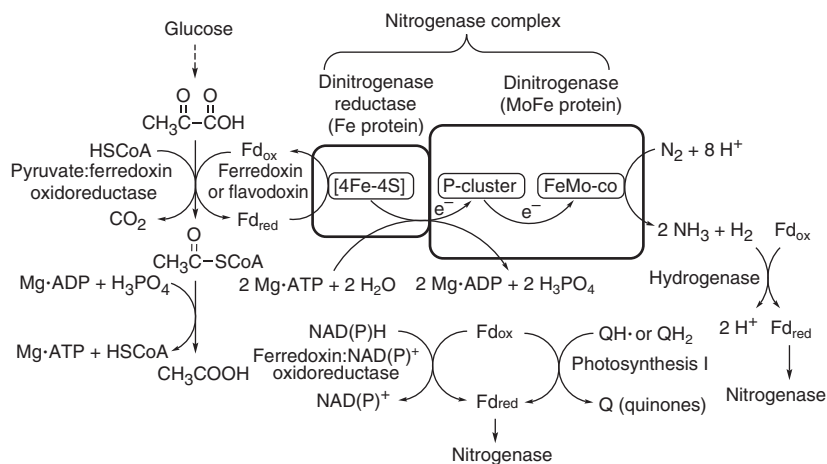


**Figure 1.6** Metabolic relationship between nitrogen fixation by Mo nitrogenase and electron transfers from pyruvate degradation, hydrogen uptake, respiration, or photosynthesis by ferredoxin/flavodoxin.

transfer an electron from the [4Fe-4S] cluster to the P-cluster, from which the FeMo-co obtains electrons [81, 82]. The rate-determining step is the dissociation of iron protein from molybdenum-iron protein ( $6 \text{ s}^{-1}$  at  $25^\circ\text{C}$ ,  $\text{pH} = 7.4$ ) [83], whereas the turnover of the formation of 1 M ammonia per molybdenum nitrogenase has been measured to be 1.5 seconds at  $23^\circ\text{C}$  by Thorneley and Lowe [84], who proposed a kinetic model of the catalytic cycle of nitrogenase reaction, where eight steps of reduction and protonation against dinitrogen occur for molybdenum nitrogenase (Figure 1.7) [64, 66, 69]. Although the amount of ATPs required for the reduction of 1 M dinitrogen has not been precisely determined by experiments, 16 ATPs are at least consumed by molybdenum nitrogenase (Figure 1.3a) based on the assumption that 2 ATPs are hydrolyzed for the transfer of one electron, whereas vanadium and iron-only nitrogenases consume at least 24 and 42 ATPs, respectively, based on the same assumption (Figure 1.3b,c) [51, 52, 55, 56]. In a typical stoichiometry by molybdenum nitrogenase, the standard transformed Gibbs energy of the reduction of dinitrogen is given as  $-667 \text{ kJ mol}^{-1}$  at zero ionic strength (Figure 1.5d) [73, 75-77].

It must be noted that both diazene ( $\text{HN}=\text{NH}$ ) and hydrazine ( $\text{H}_2\text{N}-\text{NH}_2$ ) are the substrates of nitrogenase to afford ammonia and that hydrazine is obtained as a minor product from the reduction of dinitrogen in appropriate reaction conditions [85, 86]. Without dinitrogen, protons can work as substrates to afford only dihydrogen [64]. In addition, other substrates such as ethylene, cyclopropene, acetylene, propyne, 1- or 2-butyne, allene, propargyl alcohol or amine, cyanide, cyanamide, several nitriles or isocyanides, diazirine, dimethyldiazene, carbon monoxide, carbon dioxide, carbon disulfide, carbonyl sulfide, thiocyanate, cyanate [87], nitrite, hydroxylamine [88], or azide have been known to be reduced by nitrogenase [64]. Figure 1.7 denotes the Lowe-Thorneley kinetic model modified by Hoffman and coworkers [66, 69], where formation of at least an equimolar amount of dihydrogen is inevitable for the reduction

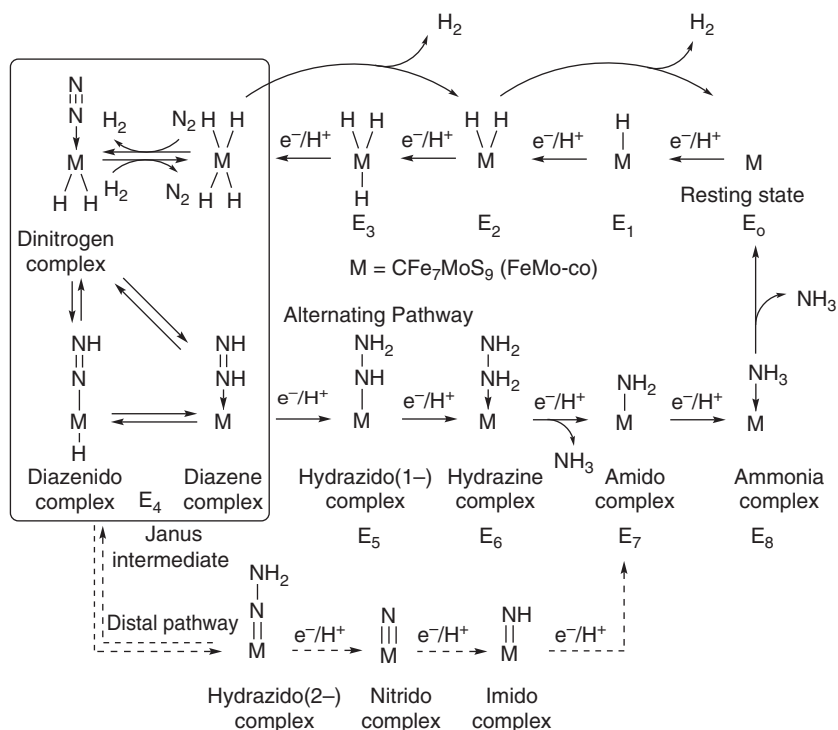


**Figure 1.7** Modified Lowe–Thorneley kinetic model of the conversion of  $\text{N}_2$  into  $\text{NH}_3$  and  $\text{H}_2$  on FeMo-co. Coordination of nitrogen- or hydrogen-containing ligands is shown as if they form mononuclear complexes, although M can be multimetallic centers and sulfur atoms where ligands may bridge or coordinate to different atoms.

of dinitrogen [89]. The first four reduction/protonation steps from  $E_0$ , the resting state of FeMo-co ( $\text{CFe}_7\text{MoS}_9$ ), give a  $(\text{CFe}_7\text{MoS}_9)(\text{H}^+)_2(\text{H}^-)_2$  species, where hydrido can bridge several transition metal centers in FeMo-co, whereas protonation likely occurs on bridging sulfur atoms. Reductive elimination of dihydrogen and coordination of dinitrogen occur in the  $E_4$  “Janus” intermediate and then pairs of reduction/protonation on dinitrogen take place to afford 2M amounts of ammonia and the starting resting  $E_0$  state. Here, the “alternating” reaction pathway where both distal and proximal nitrogen atoms are protonated stepwise and the “distal” reaction pathway where the first three protonation reactions occur at the distal nitrogen atom to give the nitrido intermediate can be drawn as shown in Figure 1.7, but the “alternating” pathway is highly likely because similar intermediates are spectroscopically observed when diazene or hydrazine is used as a reactant, and formation of hydrazine as an intermediary product is also detected.

Ferredoxin or flavodoxin, the reducing reagent of nitrogenase, transfers electrons from several metabolites, but the main source of electrons is the degradation of pyruvate for both anaerobic and aerobic microorganisms (Figure 1.6). Hydrogenase can further recycle the dihydrogen produced in nitrogen fixation, thereby minimizing the loss of energy during nitrogenase catalysis. Ferredoxin or



flavodoxin can also be reduced by NADH (nicotinamide adenine dinucleotide), NADPH (nicotinamide adenine dinucleotide phosphate), or quinones, which are produced by several metabolic pathways including both anaerobic and aerobic respiration or photosynthesis (Figure 1.6) [57–59, 90]. Cyanobacteria such as *Anabaena variabilis* perform oxygen-evolving photosynthesis and oxygen-inhibited nitrogen fixation in different cells (vegetable cells and heterocysts), or the former during day and the latter during night in the same cells, preventing the inactivation of nitrogenase by dioxygen gas [91, 92].

### 1.3 Historical Background of Transition Metal–Dinitrogen Complexes

Biological nitrogen fixation was experimentally confirmed by 1888 [93–95], and lithium was reported to react with dinitrogen at room temperature and an atmospheric pressure to form lithium nitride ( $\text{LiN}_3$ ) that can be easily converted to ammonia in 1892 [96–99]. However, formation of other nitrido complexes from the reaction dinitrogen requires higher temperature [100, 101], and further reactivities of metals with molecular dinitrogen under ambient reaction conditions have been limited in number. In 1964, Haight and Scott have reported the detection of a small amount of ammonia on prolonged cathodic reduction of dinitrogen or reduction by stannous chloride in the presence of aqueous solution of molybdate and tungstate at room temperature, although the pressure of dinitrogen gas is not well documented in the literature [102]. Conversion of dinitrogen into ammonia using transition metal complexes under ambient reaction conditions has been first reported in 1964 by Vol'pin and Shur, who obtained a small amount of ammonia when dinitrogen gas at atmospheric pressure was passed through a mixture of anhydrous  $\text{CrCl}_3$  and  $\text{LiAlH}_4$  or  $\text{EtMgBr}$  in ether at room temperature [103]. Other transition metal complexes such as  $[\text{Cp}_2\text{TiCl}_2]$  ( $\text{Cp} = \eta^5\text{-C}_5\text{H}_5$ ) or  $\text{TiCl}_4$  in combination with  $\text{EtMgBr}$  or  $i\text{Pr}_3\text{Al}$  also fixes dinitrogen [104–106]. Formation of aniline, *p*-toluidine, or aliphatic amines as a dinitrogen-derived nitrogen-containing compound has also been reported by bubbling dinitrogen through a mixture of  $[\text{Cp}_2\text{TiCl}_2]$  or  $[\text{Cp}_2\text{TiPh}_2]$ , with  $\text{PhLi}$ , *p*- $\text{TolLi}$ ,  $\text{EtMgBr}$ , or  $n\text{BuLi}$  at an atmospheric pressure and room temperature, followed by further hydrolysis [107, 108].

Isolation of a series of transition metal–dinitrogen complexes where a molecular dinitrogen is coordinated to a transition metal was first reported in 1965 by Allen and Senoff [109, 110], who performed the reduction of  $[\text{RuCl}_3(\text{H}_2\text{O})_3]$  with hydrazine hydrate in water at room temperature to afford a ruthenium–dinitrogen complex  $[\text{Ru}(\text{NH}_3)_5(\text{N}_2)]^{2+}$  in the late 1963 (Figure 1.8a) [111]. At first, they mistakenly identified that they obtained a ruthenium–hydrido complex but later found that the compound was diamagnetic with a strong infrared band around  $2170\text{--}2100\text{ cm}^{-1}$  attributable to the coordinated  $\text{N}\equiv\text{N}$  stretching, liberating dinitrogen gas on treatment with sulfuric acid.  $[\text{Ru}(\text{NH}_3)_5(\text{N}_2)]\text{Cl}_2$  also became the first transition metal–dinitrogen complex whose molecular structure was determined by a single-crystal X-ray analysis in 1966 [112].

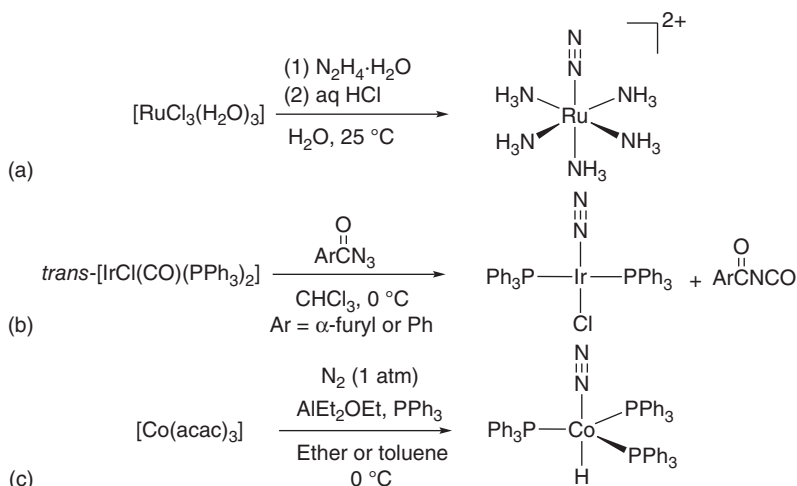


**Figure 1.8** Early reports of the preparation of transition metal–dinitrogen complexes by the reduction of metal centers in the presence of (a) hydrazine, (b) azide, and (c) dinitrogen.

The second example of transition metal–dinitrogen complexes was reported in 1966 by Collman and Kang, who obtained the iridium–dinitrogen complex *trans*-[IrCl(N<sub>2</sub>)(PPh<sub>3</sub>)<sub>2</sub>] by the reaction of Vaska’s iridium complex *trans*-[IrCl(CO)(PPh<sub>3</sub>)<sub>2</sub>] with a variety of aromatic acyl azides in chloroform at 0 °C (Figure 1.8b) [113–115].

The first transition metal–dinitrogen complex with the direct fixation of gaseous molecular dinitrogen was reported in 1967 by Yamamoto et al. who obtained the cobalt–dinitrogen complex [CoH(N<sub>2</sub>)(PPh<sub>3</sub>)<sub>3</sub>] by the reduction of [Co(acac)<sub>3</sub>] with AlEt<sub>2</sub>OEt under atmospheric pressure of dinitrogen in the presence of PPh<sub>3</sub> in ether or toluene (Figure 1.8c), which became the third example of isolated transition metal–dinitrogen complexes [116–118]. There was a confusion in the identification of its structure whether the compound contained a hydrido ligand or not, but it was later confirmed as a (hydrido)(dinitrogen) complex [119–124].

All the above three complexes are mononuclear complexes with a dinitrogen ligand coordinated to a metal center in an “end-on” manner. On the other hand, the binuclear transition metal–dinitrogen complex with a bridging dinitrogen was first reported in 1968 by Taube and coworkers, who prepared the diruthenium–dinitrogen complex *trans*-[Ru(NH<sub>3</sub>)<sub>5</sub>]<sub>2</sub>(μ-N<sub>2</sub>)]<sup>4+</sup> by the reduction of *trans*-[Ru(NH<sub>3</sub>)<sub>5</sub>Cl]<sup>2+</sup> with zinc amalgam in water under an atmospheric pressure of dinitrogen (Figure 1.9a) [125]. This compound was first identified in 1967 as the same complex with Allen and Senoff’s complex [Ru(NH<sub>3</sub>)<sub>5</sub>(N<sub>2</sub>)](BF<sub>4</sub>)<sub>2</sub>, which shows a strong IR absorption band at 2154 cm<sup>-1</sup> [109, 126], whereas a Raman band at 2100 cm<sup>-1</sup> was observed for [Ru(NH<sub>3</sub>)<sub>5</sub>]<sub>2</sub>(N<sub>2</sub>)](BF<sub>4</sub>)<sub>4</sub> [127], whose molecular structure was determined crystallographically [128].

Preparation of the heterobimetallic dinitrogen-bridged transition metal–dinitrogen complex [(PMe<sub>2</sub>Ph)<sub>4</sub>ClRe(μ-N<sub>2</sub>)MoCl<sub>4</sub>(PEtPh<sub>2</sub>)] was reported by Chatt et al. in 1969 via the ligand exchange reaction of a molybdenum phosphine

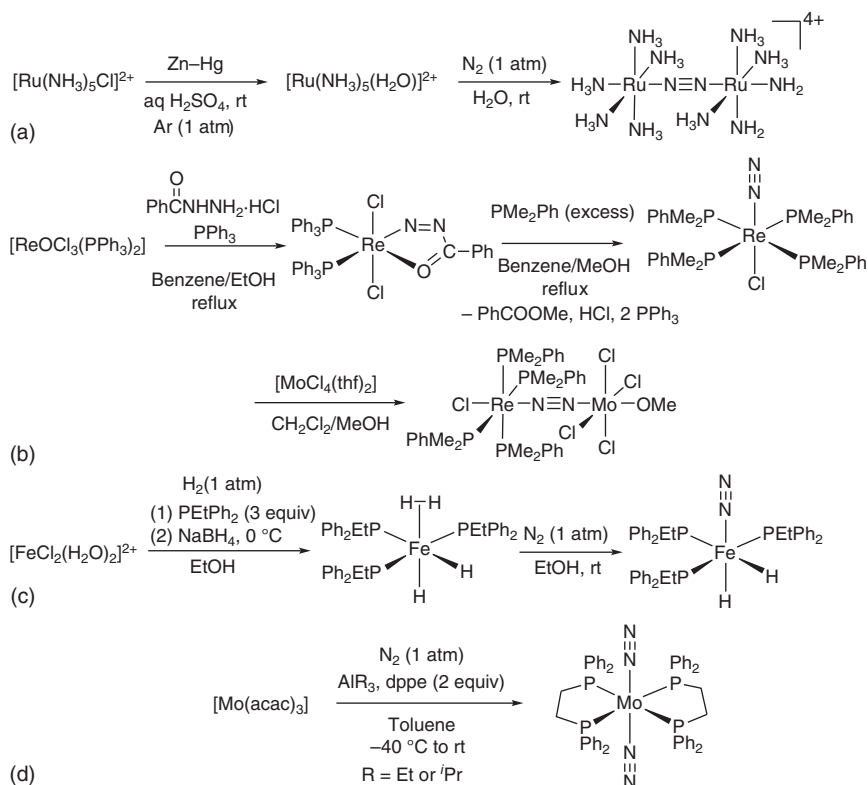


**Figure 1.9** Early reports of the preparation of transition metal–dinitrogen complexes of (a) dinuclear with bridging dinitrogen, (b) heterobimetallic dinuclear with bridging dinitrogen, (c) iron, and (d) molybdenum.

complex  $[\text{MoCl}_4(\text{PEtPh}_2)_2]$  with the mononuclear rhenium–dinitrogen complex *trans*- $[\text{ReCl}(\text{N}_2)(\text{PMe}_2\text{Ph})_4]$  [129–131], the dinitrogen ligand of which is originated from benzoylhydrazine [132–134]. The IR band attributable to the  $\text{N}\equiv\text{N}$  triple bond shifts from  $1922 \text{ cm}^{-1}$  for mononuclear rhenium complex to  $1810 \text{ cm}^{-1}$  for the heterobimetallic complex [129]. The molecular structure of its analogous complex  $[(\text{PMe}_2\text{Ph})_4\text{ClRe}(\mu\text{-N}_2)\text{MoCl}_4(\text{OMe})]$  was later confirmed by an X-ray analysis (Figure 1.9b) [135, 136]. Preparation of another heterobimetallic dinitrogen-bridged transition metal–dinitrogen complex  $[(\text{NH}_3)_5\text{-Os}(\mu\text{-N}_2)\text{Ru}(\text{NH}_3)_5]^{4+}$  was also reported in 1969 [137–140].

Preparation of iron– [141–145], molybdenum– [146–152], or vanadium–dinitrogen complexes [153–156] has been of great interest from the viewpoint of a model for the active site of nitrogenase. Sacco and Aresta reported the formation of the first iron–dinitrogen complex *cis,mer*- $[\text{FeH}_2(\text{N}_2)(\text{PEtPh}_2)_3]$  in 1968 by the reaction of dinitrogen with the dihydrogen complex *cis,mer*- $[\text{FeH}_2(\text{H}_2)(\text{PEtPh}_2)_3]$ , which was first formulated as a dihydrido complex  $[\text{FeH}_2(\text{PEtPh}_2)_3]$  [157], then reformulated as a tetrahydrido complex  $[\text{FeH}_4(\text{PEtPh}_2)_3]$  [158, 159], but later identified as the dihydrogen complex based on the  $T_1$  relaxation time measurement (Figure 1.9c) [160]. Thus, coordination of dinitrogen occurs by the

ligand exchange with a dihydrogen ligand rather than by the reductive elimination of two dihydrido ligands. The molecular structures of these complexes were later determined by X-ray and neutron diffraction studies [161].

Preparation of molybdenum–dinitrogen complex was first reported by Hidai et al. in 1969, who obtained the molybdenum–dinitrogen complex *trans*-[Mo(N<sub>2</sub>)<sub>2</sub>(dppe)<sub>2</sub>] by the reaction of [Mo(acac)<sub>3</sub>] with aluminum-reducing reagents in the presence of dppe under atmospheric pressure of dinitrogen (Figure 1.9d) [162–164]. The structure of this compound was later determined by an X-ray crystallographic analysis [165].

It is very surprising that several transition metal–dinitrogen complexes have been prepared in the late 1960s within a few years since the first discovery of transition metal–dinitrogen complexes [166–168]. Preparation and identification of dinitrogen complex of vanadium, another important transition metal of nitrogenase, was reported comparably later, when Ihmels and Rehder have reported the preparation of the anionic vanadium–dinitrogen complex [V(CO)<sub>5</sub>(N<sub>2</sub>)]<sup>−</sup> by UV irradiation of [V(CO)<sub>6</sub>]<sup>−</sup> or [V(CO)<sub>5</sub>(acetone)]<sup>−</sup> in 2-methyltetrahydrofuran at 200 K in the presence of atmospheric dinitrogen in 1985 [169, 170]. The first vanadium–dinitrogen complex crystallographically analyzed was reported in 1989 by Gambarotta and coworkers, who succeeded in the preparation of dinitrogen-bridged divanadium complex [(V{o-(Me<sub>2</sub>NCH<sub>2</sub>)C<sub>6</sub>H<sub>4</sub>}\_2(py))<sub>2</sub>(μ-N<sub>2</sub>)] (Figure 1.10a) [171].

For construction of biomimetic reactions based on the metal–sulfur clusters in metalloenzymes, a lot of sulfur-bridged transition metal clusters have been synthesized as models of nitrogenase [53, 141, 172–179], but the first dinitrogen complex [(Cp\*Ir)<sub>3</sub>{Ru(tmeda)(N<sub>2</sub>)}(μ<sub>3</sub>-S)<sub>4</sub>] (Cp\* = η<sup>5</sup>-C<sub>5</sub>Me<sub>5</sub>) where dinitrogen is coordinated to sulfur-bridged transition metal cluster has been isolated rather recently by Mizobe and coworkers (Figure 1.10b) [180, 181].

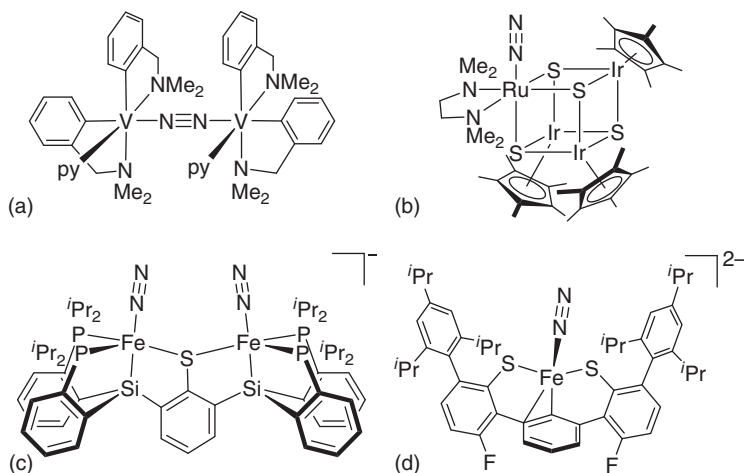


**Figure 1.10** Selected examples of transition metal–dinitrogen complexes as models for cofactors in nitrogenase: (a) vanadium–dinitrogen complex, (b) cubane–dinitrogen complex, (c) multimetallic iron–dinitrogen complex with Fe–S bonds, and (d) iron–dinitrogen complex with Fe–S and Fe–C bonds.

Isolation of the sulfur-supported multimetallic iron complex  $[\{\text{Fe}(\text{N}_2)\}_2(\mu\text{-SAr})]^-$  ( $\text{Ar} = 2,5\text{-C}_6\text{H}_4\{\text{Si}(\text{C}_6\text{H}_4\text{P}^i\text{Pr}_2\text{-}o)_2\}_2$ ) has also been reported more recently by Creutz and Peters (Figure 1.10c) [182].

Recent analyses of nitrogenase have clarified that FeMo-co contains a carbide atom that constitutes the edge of two cuboidal clusters ( $[\text{Fe}_4\text{S}_3]$  and  $[\text{Fe}_3\text{MoS}_3]$ ) [60–62], where the carbon atom has been transferred from the methyl radical originated from *S*-adenosylmethionine to bridge the two clusters [183]. The iron–dinitrogen complex  $[\text{Fe}(\text{N}_2)(\text{L})]^{2-}$  ( $\text{LH}_2 = 6,6''\text{-F}_2\text{-}3,3''\text{-(}2,4,6\text{-}i\text{Pr}_3\text{C}_6\text{H}_2)_2\text{-}m\text{-terphenyl-}2,2''\text{-(SH)}_2$ ) bearing both Fe–S and Fe–C bonds has been prepared by Holland and coworkers in 2015 (Figure 1.10d) [179, 184].

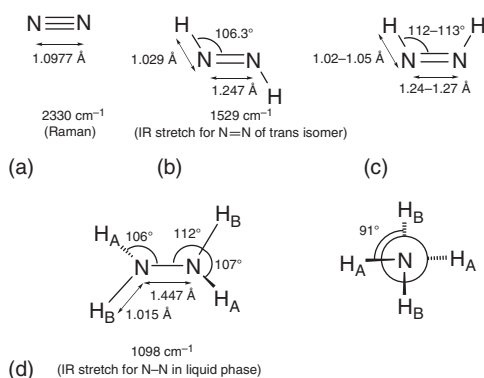
## 1.4 Coordination Chemistry of Transition Metal–Dinitrogen Complexes

### 1.4.1 Coordination Patterns of Dinitrogen and Mononuclear Transition Metal–Dinitrogen Complexes

Dinitrogen is a diatomic molecule with a Raman band at 2330, 2291, or 2252  $\text{cm}^{-1}$  for gaseous  $^{14}\text{N}_2$ ,  $^{14}\text{N}^{15}\text{N}$ , or  $^{15}\text{N}_2$ , respectively, because of the stretching vibration of the  $\text{N}\equiv\text{N}$  triple bond [185, 186]. The interatomic distance between two nitrogen atoms has been measured to be ranging from 1.09 to 1.11 Å by X-ray analyses of several different phases of solid-state dinitrogen ( $\alpha$ -,  $\beta$ -,  $\gamma$ -, and  $\delta$ - $\text{N}_2$ ) at very low temperatures or at extremely high pressures [187–198], whereas that of gaseous molecular dinitrogen calculated based on the spectroscopic data for the electronic ground state is 1.0977 Å (Figure 1.11a) [199, 200].

Three isomers are known for diazene or diimine: *trans*-diazene (Figure 1.11b), *cis*-diazene (Figure 1.11c), and isodiazene ( $\text{H}_2\text{N}^+=\text{N}^-$ ) [201, 202]. *trans*-Diazene is the most stable isomer among them, but *cis*-diazene, only 21  $\text{kJ mol}^{-1}$  higher in enthalpy than *trans*-diazene [202, 203], works as a hydrogenation reagent against unsaturated compounds with stereoselective syn addition of  $\text{H}_2$  [204] and is also regarded as an intermediary structure of the reduction of dinitrogen in nitrogenase reactions [205]. The interatomic distance between two nitrogen atoms in *trans*-diazene has been determined to be 1.247 Å based on the UV and

**Figure 1.11** Molecular structures of (a)  $\text{N}_2$ , (b) *trans*- $\text{N}_2\text{H}_2$ , (c) *cis*- $\text{N}_2\text{H}_2$ , and (d)  $\text{N}_2\text{H}_4$ .



IR spectroscopies (Figure 1.11b) [206, 207], whereas spectroscopic observations for *cis*-diazene that has not been isolated in the pure form have been problematic [208]. The bond lengths and angles of *cis*-diazene shown in Figure 1.11c are those taken from theoretical calculations [203, 209, 210].

The melting point of free hydrazine is not low (+1.4 °C), and the solid-state structure was analyzed by an X-ray analysis, which gave the N–N bond length at 1.46 Å at –15 °C [211], whereas the electron diffraction studies and microwave spectroscopies gave the N–N bond distance at 1.447 Å (Figure 1.11d) [212–215]. The Raman and IR spectra give the stretching vibration for N–N in the range of 1076–1126 cm<sup>-1</sup>, which can vary according to the phases of hydrazine (gas, liquid, or solid) [216–220]. It must be noted that the dihedral angle of the H–N–N–H is almost 90° because of the existence of lone pairs of nitrogen atoms, suggesting that the bond order of N–N in hydrazine is one. Based on the crystallographic data of compounds containing N–N bonds, bond distances of 1.10, 1.22, and 1.46 Å as reference values for triple-, double-, and single-bond orders are proposed [221].

Since 1965, a lot of transition metal–dinitrogen complexes have been prepared [166–168, 221–231], including both mononuclear dinitrogen complexes and dinitrogen-bridged multinuclear complexes. General bonding modes of dinitrogen in mononuclear and dinuclear transition metal–dinitrogen complexes are summarized in Figure 1.12a [221, 227].

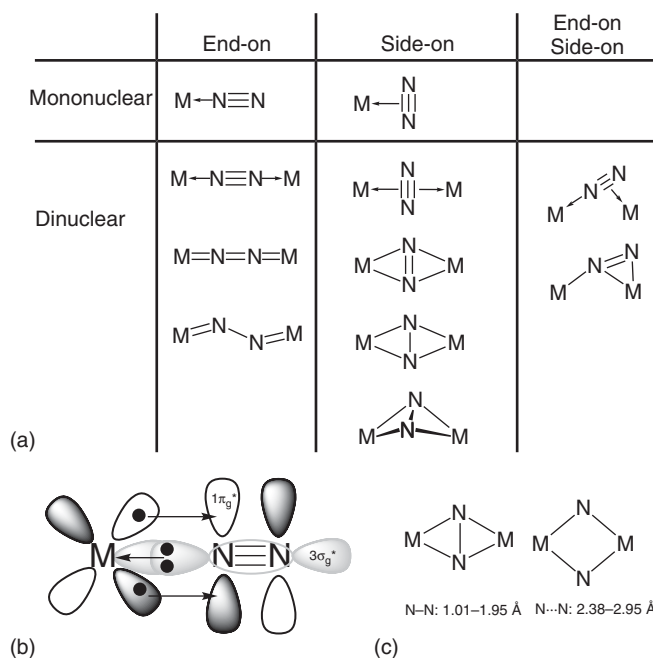


**Figure 1.12** (a) General bonding modes of dinitrogen in mononuclear and dinuclear transition metal–dinitrogen complexes. (b) Schematics of molecular orbital interactions of mononuclear end-on-bound transition metal–dinitrogen complex. (c) Metric difference of side-on-bridged dinuclear transition metal–dinitrogen complexes and bis(nitrido)-bridged complexes.